Solid Oxide Membrane Process for Magnesium Production Directly from Magnesium Oxide

A. KRISHNAN, X.G. LU, and U.B. PAL

The solid oxide membrane (SOM) process is an emerging technology for the environmentally friendly extraction of high-energy-content metals such as magnesium, tantalum, and titanium directly from their respective oxides. This paper reports on the recent success of the SOM process for magnesium production from magnesium oxide dissolved in fluoride-based fluxes in the temperature range 1150 °C to 1300 °C. This process employs an inert oxygen-ion-conducting stabilized zirconia membrane to separate the inert cathode in the flux from the anode. When the applied electrical potential between the electrodes exceeds the dissociation potential of magnesium oxide, oxygen ions are pumped out of the melt and through the zirconia membrane to the anode where they are oxidized. Reduced magnesium evolves at the cathode as a vapor and is condensed in a separate chamber yielding a high-purity product. The SOM cell has been electrochemically characterized, and key concepts related to MgO dissociation, leakage current, and mass transfer relevant to the SOM process are explained.

I. INTRODUCTION

MAGNESIUM is the third most abundant metal in the earth's crust after aluminum and iron and is widely distributed in almost all parts of the world as oxides, carbonates, sulfates, chlorides, and their combinations. It constitutes 2 wt pct of the earth's crust and is the third most plentiful element dissolved in seawater with a concentration averaging 0.13 wt pct.[1] Magnesium has been primarily used as an addition in aluminum alloys, for desulfurization of steel and production of ductile cast iron. Recently, magnesium has been gaining attention as a material for use in next generation vehicles with an emphasis on weight reduction.[2] The price of magnesium dictated by its existing primary production processes has been a major barrier to its more extensive use in the automobile industry. For the future hydrogen economy, magnesium hydride slurry is being investigated as a potential medium for hydrogen storage in the form of a pumpable slurry.[3] Hydrogen is generated when needed by hydrolysis of magnesium hydride. The by-product of the hydrolysis reaction is stable magnesium hydroxide. The magnesium hydride slurry technology lends itself well for automotive applications in conjunction with fuel cells. For such high volume applications, the success and long-term economic viability depends on an efficient and cost-effective recycling scheme for converting magnesium hydroxide into magnesium.

Two major production routes currently exist for primary magnesium: metallothermic reduction and the direct electrolysis of magnesium chloride from a chloride bath at 675 °C to 800 °C.[4] The metallothermic process for producing magnesium is based on the thermal reduction of calcined dolomite or magnesite at high temperature (1200 °C to 1400 °C) and reduced pressure with ferrosilicon as the reductant. The reduced magnesium vapor is collected in an attached condenser. The ferrosilicon reductant represents 12 KWh/kg or roughly 40 pct of the total energy required to produce magnesium and roughly a third of its total production cost. Furthermore, this batch process generates about 4 to 5 tons of slag per ton of magnesium, which must be properly disposed. The conventional electrolytic magnesium process is based on an anhydrous chloride feed material that is recovered from brines *via* an elaborate and expensive front-end dehydration process. The feed preparation process can represent 80 pct of the plant footprint and 30 pct of its capital cost.[4] Anhydrous magnesium chloride for electrolysis can also be produced *via* high-temperature carbochlorination of oxide magnesium ores,[5] but this process is also relatively costly. Electrolysis of anhydrous chloride generates chlorine gas at the graphite anode that can represent an environmental concern if improperly handled, thus requiring additional capital and operating resources. Conventional technologies for the production of magnesium are energy and materials intensive and pose several environmental and health risks. The price and market potential of magnesium metal justify the research and development of new technology that can reduce both cost (capital and operating) and adverse environmental impact.

Electro-deoxidation of metals and alloys and electrochemical reduction of oxides have been studied by many workers over the years. Two major approaches have been considered. The first involves use of a solid-ceramic-ion-conducting membrane having permeability (conductivity) for a specific ion. This approach is relevant to this paper and is discussed later in greater detail. The second approach does not employ an ion selective membrane, but instead involves ionization or electrochemically depositing a reactive metal such as calcium from calcium chloride melts onto an oxide or metal cathode, thereby deoxidizing it. These approaches have been used to deoxidize titanium[6] and yttrium,[7] refine molten copper,[8] and reduce TiO_2,[9,10] niobium pentoxide,[11] chromium oxide,[12] and silica.[13] For such reduction of metal oxides with calcium, the process gets rate limited by oxygen transport in the reduced solid metal that surrounds the oxide. Calcium metal generated at the cathode during electrochemical reduction can dissolve in calcium chloride melts, resulting in a decrease in current efficiency.

A. KRISHNAN, Graduate Student, and U.B. PAL, Professor, are with the Manufacturing Engineering Department, Boston University, Boston, MA 02446. Contact e-mail: upal@bu.edu X.G. LU, Visiting Professor, Manufacturing Engineering Department, Boston University, is on leave from Department of Materials and Engineering, Shanghai University, Shanghai, P.R. China 200072.

Manuscript submitted December 10, 2004.

Since Kiukola and Wagner,[14] many researchers have used stabilized-zirconia-based electrochemical cells to refine melts. Some researchers[15,16,17] have used an electrolytic method to remove oxygen from copper melts, while others have used a galvanic method to deoxidize iron[18,19] and copper melts.[20] These attempts to deoxidize molten metals have not been commercialized because high current densities could not be achieved in the process. The transport of oxygen to the membrane/melt interface from the bulk becomes rate controlling and ultimately limits the final oxygen content in the melt.

Ion-specific membranes have been proposed to extract metals from their dissociable salts. These membranes can be divided into cation-specific membranes (β-alumina for Na) and anion-specific membranes (stabilized zirconia for oxygen ions). Kummer[21] was the first to suggest the use of a cation-specific membrane to separate metal from its electrically dissociable salt. By applying a potential exceeding the dissociation potential of the metal salt, the cations from the melt containing the dissociable salt are driven across the solid cation-specific ceramic membrane such as Na in β-alumina to the cathode to produce the metal. Minck[22] later proposed a modification of Kummer's apparatus in order to prevent the degradation of the solid electrolyte membrane. For anion-specific membranes, Marincek was the first to propose a method[23] and apparatus[24] for electrolysis of metal oxides using a thin layer of an oxygen-ion-conducting membrane such as zirconia. Sammells[25] later proposed a similar method for dissociating alkali oxides to produce oxygen gas and liquid alkali metal (such as lithium) in a high-temperature electrolytic cell for lunar applications. In this method disclosed by Sammells, the process relies on high lithium cation mobility to drive the reaction. Pal[26,27] has pointed out that the diffusivity of the anion in the molten flux should exceed 10^{-5} cm^2/s so that the transport of the anion through the flux and to the flux/membrane interface is not rate limiting. This is to ensure that the flux/membrane interface does not get polarized. Pal *et al.*[28] described a method for the electrochemical recovery of metals from slag using a galvanic (current producing) cell in which no external electric potential is applied. The refining process is driven by the chemical-potential gradient between the oxygen within the slag and a refining gas that is separated from the slag by a solid oxygen-ion-conducting electrolyte. Since the oxygen chemical potential is fixed in the refining gas, large current densities cannot be obtained and therefore the cell is not well suited for extracting the desired metal from its oxide on an industrial scale.

Rapp[29,30] later considered a modification of a nonconsumable solid oxide fuel cell (SOFC)–type anode for the Hall Héroult cell (HHC) for electrowinning of aluminum. Use of a nonconsumable anode would lead to a confined anodic reduction site, providing significant reductions in cell potential, cost of anode, and release of greenhouse gases. However, detailed studies of the solubility of alumina, zirconia, and yttria over a very wide range of cryolite bath ratios showed that no bath composition exists where alumina would be sufficiently soluble while the solid electrolyte components were sufficiently insoluble. On further investigation, Rapp and Zhang[31] have proposed an alternative flux system based on fused sodium sulfate as a replacement for cryolite for electrowinning of aluminum in the HHC. Lacamera[32] has proposed electrolysis of metal oxide dissolved in a molten salt containing at least one chloride and one fluoride, specifically related to the production of aluminum from alumina. Use of a mixed fluoride-chloride flux in the HHC is advantageous in terms of lowering operating temperatures and improving cell productivity and efficiency. In order to employ mixed fluoride-chloride molten fluxes, a solid oxide ion conductor will be required to separate the flux from the anode. This arrangement is critical in order to prevent formation of chlorofluorocarbons at the anode. In all of these applications of solid-oxygen-ion-conducting membranes, high current densities (>1 A/cm^2) could not be obtained through the membrane and the cell.

This paper reports on the success of solid oxide membrane (SOM) process to extract magnesium directly from magnesium oxide. Ten weight percent magnesium oxide dissolved in a suitable fluoride-based flux is reduced in a SOM cell in the temperature range of 1150 °C to 1300 °C. The possibility of operating the cell at high current densities is also discussed.

II. SOM PROCESS

The fundamental configuration of the SOM process is shown in Figure 1. It consists of a solid-oxygen-ion-conducting stabilized-zirconia electrolyte (membrane) that separates the anode from the melt containing the oxide of the metal to be reduced. If the membrane in contact with the melt is inert, then it can be viewed as part of an inert-anode structure. An inert cathode is placed in the melt. When the applied electric potential between the anode and the cathode exceeds the dissociation potential of the oxide to be reduced, the desired metal cations are reduced at the cathode, and the oxygen ions migrate through the membrane and are oxidized at the anode.

The full benefit of the proposed SOM process can be realized if the process is conducted at temperatures between 1100 °C and 1300 °C. At these temperatures, the ohmic resistance drop across the stabilized zirconia membrane is low, and an appropriate fluoride-based flux can be chosen that has high ionic conductivity, high oxide solubility, and low viscosity. So, with adequate flux stirring, the overall resistance in the cell can be lowered and high current densities of the order of 1 A/cm^2 or greater can be obtained by increasing the applied potential. It is important to note that the flux used should have negligible solubility for the membrane oxides. Otherwise, it will also result in the dissolution and reduction of membrane oxides. Since the temperature is above

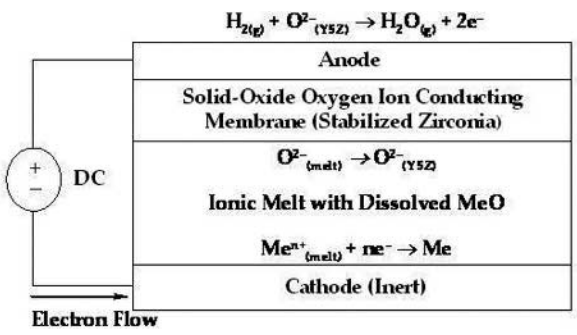

Fig. 1—Fundamental configuration of the SOM cell.

1100 °C, the process efficiency can be further increased by directly reforming hydrocarbon fuel over the anode. It may be noted that several attempts have been made at employing the solid-oxygen-ion-conducting membrane as part of an inert anode at temperatures below 1000 °C. However, these efforts have not been successful in developing a commercial process[22,24,25,33] mainly because sufficiently high current densities could not be obtained through the membrane and the flux used was reactive with the membrane.

This process is different from commercial molten salt electrolysis technologies, as only oxygen ions are allowed to pass across the SOM from the molten flux to the anode. As a result, only oxygen is oxidized at the anode. Therefore, metal oxides can be dissolved in relatively low melting point halide-based fluxes without the concern of producing halide gases or oxy-halide-hydrocarbon compounds at the anode. This eliminates many of the significant environmental concerns associated with conventional high-temperature molten salt electrolytic processes. It also offers the flexibility to directly process as-mined ores and synthesize commonly used alloy compositions. The SOM process is an emerging generic technology for the extraction of metals and alloys directly from their respective metal oxides. It may offer a viable, cost-effective, and cleaner alternative to existing magnesium extraction processes.

A. *Transport in SOM Cell during Electrolysis*

The experimental SOM cell described later is of the following type.

1. *C/Cu(l)/yttria-stabilized zirconia/ionic flux with dissolved MgO/steel*

Liquid copper (Cu(l)) is used as a medium to transport oxygen from the YSZ/copper interface to graphite where it is oxidized. Dissolved oxygen ($[O]_{Cu}$) has high solubility and diffusivity in liquid copper, as measured by Oberg *et al.*[34] The diffusivity (D_O^{Cu}) and solubility (weight percent) of dissolved oxygen in copper in the temperature range of 1000 °C to 1350 °C are

$$D_O^{Cu} = 6.19 \times 10^{-3} \exp\left(\frac{-12{,}900}{RT}\right) \text{cm}^2/\text{s} \qquad [1]$$

$$[O]_{Cu}\,(\text{wt pct}) = (P_{O_2})^{\frac{1}{2}} \exp\left(\frac{10{,}859}{T} - 2.66\right) \qquad [2]$$

The liquid copper and graphite will be henceforth referred to as the extended anode. When the applied potential exceeds the dissociation potential of magnesium oxide, the transport of oxygen and magnesium ions in the cell can be given by the following.

2. *Oxygen ion (O^{2-})*

(1) Transport of O^{2-} from the bulk flux (O^{2-}_{flux}) to the flux/YSZ interface.
(2) Transport of O^{2-}_{flux} across the flux/YSZ interface ($O^{2-}_{flux} \rightarrow O^{2-}_{YSZ}$).
(3) Transport of O^{2-}_{YSZ} through the YSZ membrane to the YSZ/molten copper interface.
(4) Electrochemical reaction (oxidation) of O^{2-}_{YSZ} at the YSZ/molten copper interface ($O^{2-}_{YSZ} \rightarrow [O]_{Cu} + 2e^-$).
(5) Transport of oxygen dissolved in copper ($[O]_{Cu}$) from the YSZ/molten copper interface to the graphite/molten copper interface.
(6) Reaction of $[O]_{Cu}$ at the graphite/molten copper interface resulting in evolution of carbon monoxide ($[O]_{Cu} + C \rightarrow CO(g)$).

3. *Magnesium ion (Mg^{2+})*

(7) Transport of Mg^{2+} from the bulk flux (Mg^{2+}_{bulk}) to the flux/cathode interface.
(8) Electrochemical reaction (reduction) of Mg^{2+}_{bulk} at the flux/cathode interface resulting in the evolution of magnesium vapor ($Mg^{2+}_{bulk} + 2e^- \rightarrow Mg(g)$).

Steps 1 through 6 and steps 7 and 8 occur in series and the slowest step ultimately determines the overall metal production rate in the SOM cell. The oxygen ion conductivity ($k_{O^{2-}}$) of the 6 mol pct yttria-stabilized zirconia (YSZ) membrane used for experiments and measured by the four-probe DC conductivity method was 0.1 to 0.19 S/cm between 1150 °C and 1300 °C. Since the process is restrained by the use of a certain minimum thickness of zirconia membrane, it is desirable to engineer/optimize the SOM electrolysis process so that transport of oxygen ions through the zirconia membrane (step 3) is rate controlling. The flux is an electron blocker and ionic resistance of the flux is much smaller than that of the zirconia membrane. Adequate stirring of the melt and having sufficient MgO in the flux are essential to ensure that steps 1 and 7 are not rate controlling. The flux must completely wet zirconia so that step 2 is not rate controlling. The temperature must be maintained sufficiently high (≥1100 °C) so that charge transfer reactions are not rate controlling (steps 4 and 8). Since the oxygen solubility and diffusivity are high in molten copper, step 5 will not be rate controlling if the molten copper is well stirred by CO(g); the reaction in step 6 has a high negative free energy change.[35] These steps are further analyzed in the section on mass-transfer analysis. The individual half-cell reactions are as follows:

At the cathode,

$$Mg^{2+} + 2e^- \rightarrow Mg(g)$$

At YSZ/copper interface,

$$O^{2-} = [O]_{Cu} + 2e^-$$

At extended anode,

$$C + [O]_{Cu} = CO(g)$$

Overall cell reaction can be given as

$$Mg^{2+} + C + O^{2-} = Mg(g) + CO(g)$$

$$MgO + C = Mg(g) + CO(g)$$

III. EXPERIMENTAL AND RESULTS

Proof of concept for the magnesium SOM process has been demonstrated using a high-temperature flux system (HTF: MgF_2-10 wt pct MgO at 1300 °C) and a low-temperature flux system (LTF : (55.5 wt pct MgF_2-CaF_2)-10 wt pct MgO at 1150 °C). Previously reported SOM cells[36] were exploratory in nature and intended to refine the SOM cell design while producing small amounts of magnesium (less than 3 g).

A. *Chemicals and Materials*

Magnesium fluoride (99.5 pct), calcium fluoride (99.7 pct), and magnesium oxide (99 pct) used to prepare the flux were supplied by Alfa Aesar (Ward Hill, MA). The powders were dried overnight at 200 °C, weighed, and mixed according to the required flux chemistry. The mixed powders were premelted in a graphite crucible under an argon environment. The premelted flux was then crushed into a coarse powder and used for the experiments. High-density graphite rod (0.6-cm o.d.) from graphite engineering (Greenville, MI) was used as a consumable anode. A closed one end (1.9-cm o.d., 1.42-cm i.d., 20-cm long) yttria-stabilized zirconia tube (6 mol pct Y_2O_3) from Vesuvius McDanel (Beaver Falls, PA) was used as the membrane.

B. *Experiments*

An electrolytic cell and magnesium collection apparatus have been designed to produce and contain 100 to 200 g of magnesium metal. The electrolytic cell shown in Figure 2 can use up to 33 cm^2 of anode area, operate at current densities as high as 1 A/cm^2, and produce as much as 15 g of magnesium per hour. The setup was validated by running the cell at 3 to 4 V for an extended period (5 to 10 hours) by employing 15.2 cm^2 of anode area and collecting 15 to 25 g of magnesium.

Nearly all of the setup with the notable exception of the YSZ membrane and extended anode (graphite and liquid copper) is constructed of 304 stainless steel. The YSZ membrane is held in position using alumina spacers cemented together with alumina cement (Figure 2). The entire apparatus is contained and heated within the mullite reaction tube of a molybdenum disilicide resistance furnace. The upper electrolysis chamber shown is 6 inches in length, and is positioned so that the melt remains in the hot zone of the furnace. The apparatus takes advantage of the natural temperature gradient of the resistance furnace such that the electrolysis chamber is either maintained at 1150 °C (for LTF) or 1300 °C (for HTF), while the lower condensation chamber is positioned such that the temperature within the chamber varies from 1100 °C to 500 °C. In order to protect the YSZ membrane above the flux from the Mg vapor that is produced along the wall of the stainless steel container (cathode), argon gas is introduced into the chamber as a carrier gas and diluent. The dilution of magnesium vapor by argon is required to reduce the partial pressure of magnesium vapor in the SOM reactor in order to ensure stability of the zirconia membrane (Figure 3). The argon-magnesium gas mixture passes out of the electrolysis chamber to the lower condensation chamber, which can be maintained at a temperature such that magnesium is collected as either a liquid or solid. The remaining argon gas then passes through a baffle and exits the condensation chamber through the bottom of the furnace. In some experiments, the tube carrying the argon gas to dilute the Mg vapor is extended into the melt with the goal of improving mass transfer in the melt.

The entire setup placed inside a gas tight mullite tube is heated to the desired temperature at the rate of 3 °C/min. High-purity argon (250 cc/min) is passed through the mullite tube to generate an inert atmosphere around the setup. The exit gas is continuously monitored using a zirconia-based-oxygen sensor. After equilibrating at the desired temperature for 1 hour, the cell is characterized using impedance spectroscopy, potentiodynamic sweeps, and potentiostatic holds. The electrochemical instrumentation consisted of a Princeton Applied Research (PAR) (Oak Ridge, TN) potentiostat (model 263 A) and Solartron impedance analyzer (Houston, TX) (model 1250 B). A KEPCO (Flushing, NY) power booster was used to increase the current limit of the potentiostat to 10 A. Data acquisition and control of the above instruments was achieved with CorrWare® and Zplot® (software) from Scribner Associates (Southern Pines, NC). A Hewlett-Packard (Palo Alto, CA) power supply (model 6033A) was used to apply a constant potential to the cell for electrolysis. The SOM cell showed a very small open circuit potential (<10 mV), indicating that the initial oxygen chemical potentials at the anode and the cathode were nearly equal. The applied electrical potential and resulting current from the cell were logged at 1-second intervals using a Fluke (Everett, WA) Hydra® data logger (model 2635A).

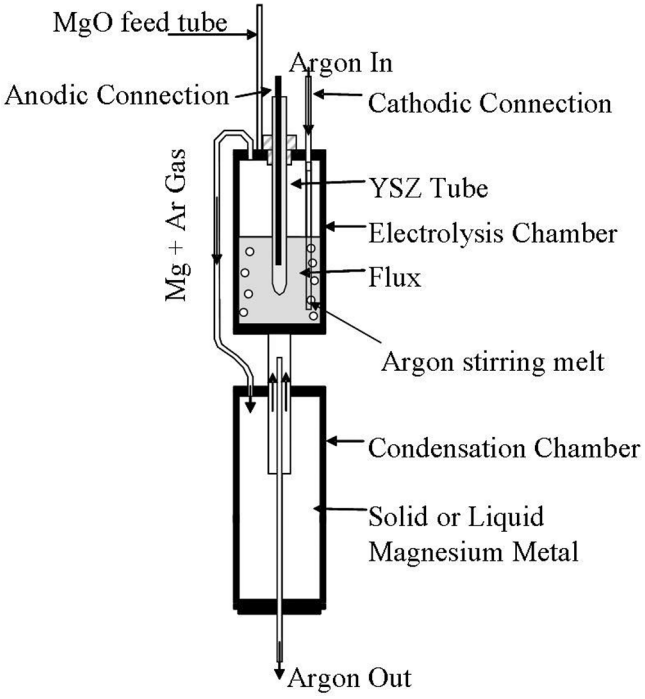

Fig. 2—Experimental setup for electrolysis by the SOM process.

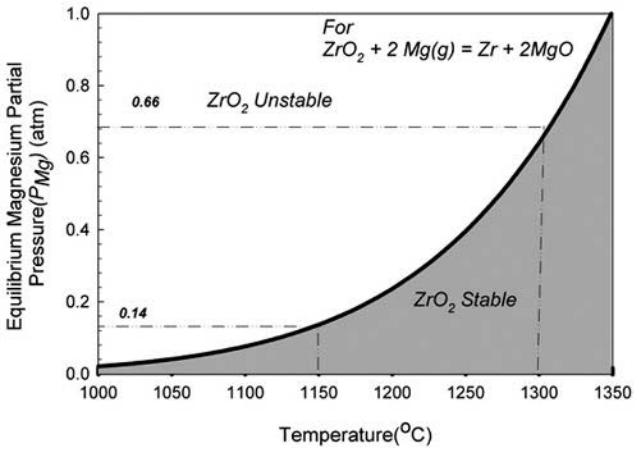

Fig. 3—Effect of partial pressure of magnesium vapor in the electrolysis chamber on the stability of the zirconia membrane.

1. *High-temperature flux system*

In this system, as per the pseudobinary magnesium fluoride–magnesium oxide phase diagram, 10 wt pct magnesium oxide was dissolved in magnesium fluoride.[37] At 1300 °C, the dissociation potential of magnesium oxide in this system has been measured to be approximately 0.59 V (Figure 4). The leakage current (current prior to MgO dissociation) makes it difficult to exactly identify the dissociation potential; the source of the small leakage current is discussed later in the paper. Therefore, the dissociation potential is identified by extending the smaller leakage current slope and the higher ionic current slope of the I-V response, as depicted now in Figure 4. It should be noted that the dissociation potential does not have much practical significance as the cell is operated at much higher potentials. Using a fast (5 mv/s) potentiodynamic sweep (Figure 5), an anodic current density of 0.55 A/cm^2 was achieved when a potential of 4 V was applied between the anode and cathode. The total ohmic resistance of the cell measured by alternating current (ac) impedance spectroscopy[38] was between 0.27 and 0.29 ohms. For instance, when a current of 8 amperes was measured through the cell, as depicted in Figures 5 and 6, the voltage drop across the cell corresponding to the ohmic resistance was 2.16 to 2.32 V. This implies that the potential used to dissociate MgO and other losses in the cell was 1.68 to 1.84 V. Since a diffusion-limited current is not observed, it is possible to obtain a current density of 1 A/cm^2 with adequate stirring and applying a larger potential (6 V). The SOM cell with the HTF system was held at a constant voltage of 4 V for 5.25 hours. Figure 6 shows the cell current as a function of time during this period. During this period, the MgO concentration decreased from 10 to 5 wt pct and this is reflected by the gradual decay in current. The initial increase and instability in the current resulted during adjusting the depth of the graphite rod in the copper melt. During the experiment, 15.2 cm^2 of anode area was used and 35.58 ampere-hours of charge were passed through the system. This is obtained by integrating the area under the total current versus time plot in Figure 6. At near 100 pct Faradic efficiency, this would theoretically produce 16.13 g of magnesium. Following the completion of this experiment, the condensation chamber was disassembled for inspection. The bright metallic coating inside the condenser (shown in Figure 7) was magnesium metal, which condensed directly from the gas to solid phase. The deposit was analyzed by energy-dispersive X-ray (EDAX) and found to be pure magnesium (within the detection limits of the instrument). The approximate weight of the metal deposited (15 to 16 g) was found to correspond well with the theoretical estimate per Faraday's law.

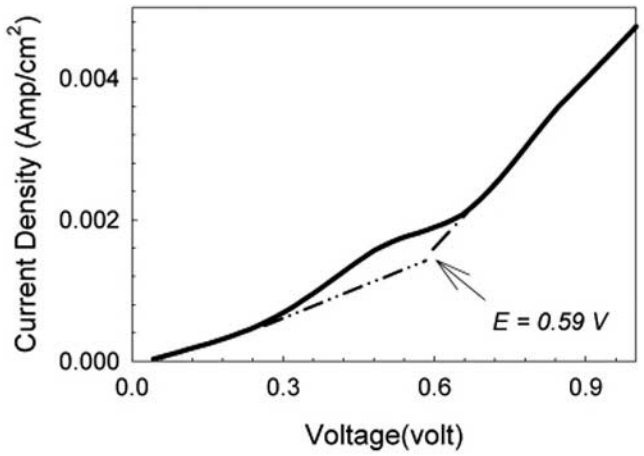

Fig. 4—Slow potentiodynamic scan (0.5 mv/s) to estimate dissociation potential of magnesium oxide in the HTF system.

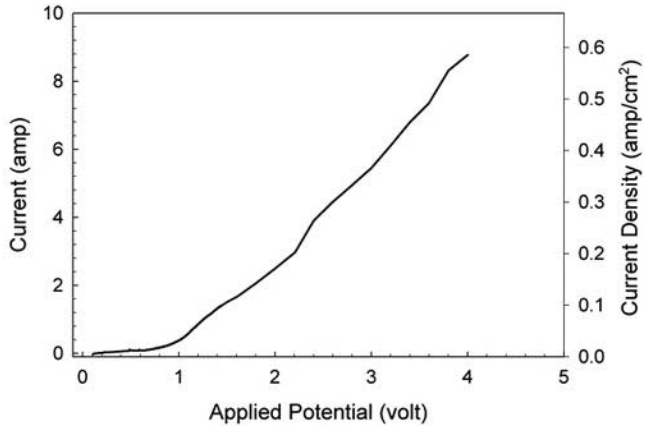

Fig. 5—Fast potentiodynamic scan (5 mv/s) in the HTF system.

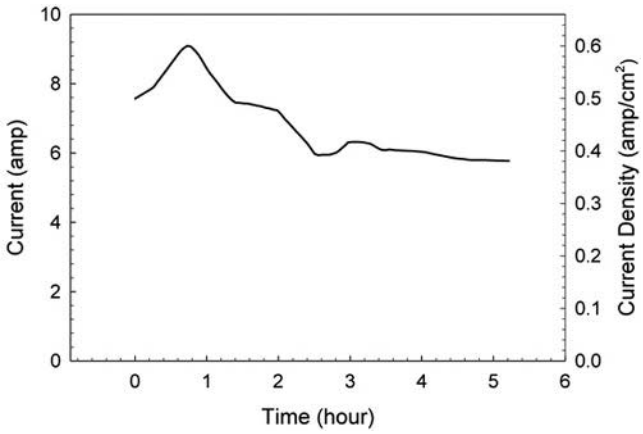

Fig. 6—Current response during electrolysis with 4 V in the HTF system.

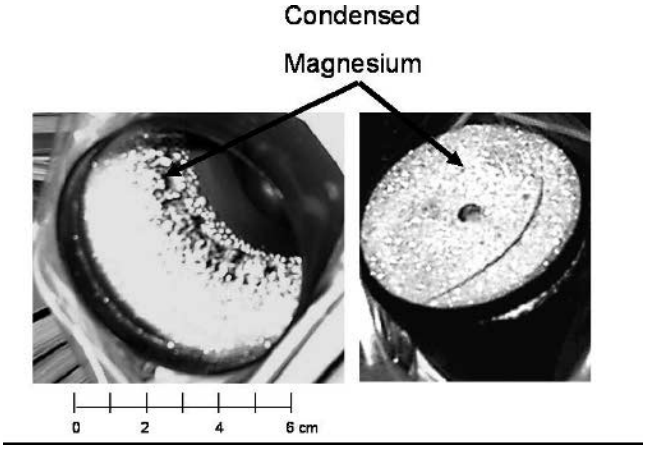

Fig. 7—Sidewall and bottom surfaces of the lower condensation chamber.

2. *LTF system*

In the LTF system, 10 wt pct magnesium oxide was dissolved in a eutectic composition of the magnesium fluoride-calcium fluoride flux.[39] The cross section of the quenched slag indicated homogenous dissolution of MgO. From Figure 8, with a slow (0.5 mv/s) potentiodynamic sweep, the dissociation potential for magnesium oxide in the flux at 1150 °C was determined to be 0.63 V. Once again, the dissociation potential is identified by extending the smaller leakage current slope and the higher ionic current slope of the I-V response. During a slow potentiodynamic scan (Figure 9), the current through the cell steadily increases, indicating that higher current densities (0.8 to 1 A/cm^2) are possible since a diffusion-limited current was not observed. The SOM cell was evaluated for a period of 20 hours. During this time, 3 V was applied for 12 hours to produce magnesium from magnesium oxide. The remainder of the time was spent in electrochemically characterizing the cell. A total of 39.6 ampere-hours were passed through the cell at 3 V using 15.2 cm^2 of the anode area, theoretically reducing 17.95 g of magnesium. The current response at 3 V can be seen from Figure 10. The gradual decay in current is due to decreasing MgO concentration from 10 to 6 wt pct during the experiment. The cell impedance was measured periodically and was observed to be constant (typically, 0.22 ohms) (Figure 11). Although the temperature is lower, the cell impedance measured in LTF is slightly less than that measured in the HTF system. This is probably due to the different flux system chosen and temperature relative to the eutectic. The condenser showed the magnesium deposit as solid lumps and fine crystals (Figure 12). The fine crystals are deposited at colder parts of the condenser, while the lumps are seen closer to the top of the condenser that was hotter (Figure 12(a)). The EDAX spectrum (Figure 12(b)) of the Mg deposited with the LTF flux system shows no detectable Ca in the Mg deposit even though the flux contained CaF_2. The approximate weight of the magnesium deposited (17 to 18 g) once again was found to correspond well with the theoretical estimate per Faraday's law, thus indicating a high Faradic efficiency for the process. After the experiment, the YSZ membrane in contact with the flux was sectioned, polished, and examined by optical microscopy. The microstructure of the as-received membrane and membrane after the 20 hours experiment is compared in Figure 13. The membrane in Figure 13(b) appears to be essentially unaffected by the experiment.

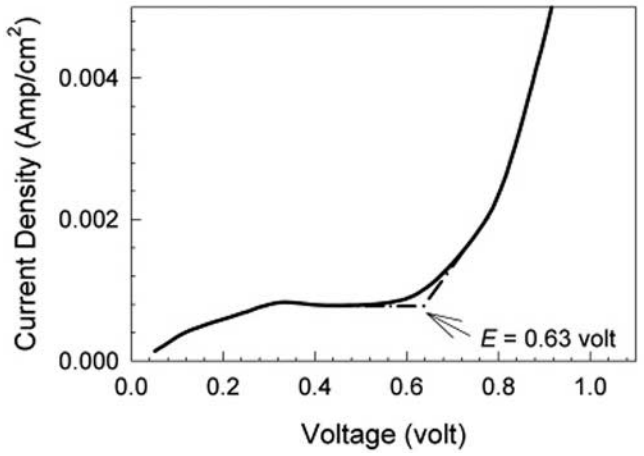

Fig. 8—Slow potentiodynamic scan (0.5 mv/s) to estimate dissociation potential of magnesium oxide in the LTF system.

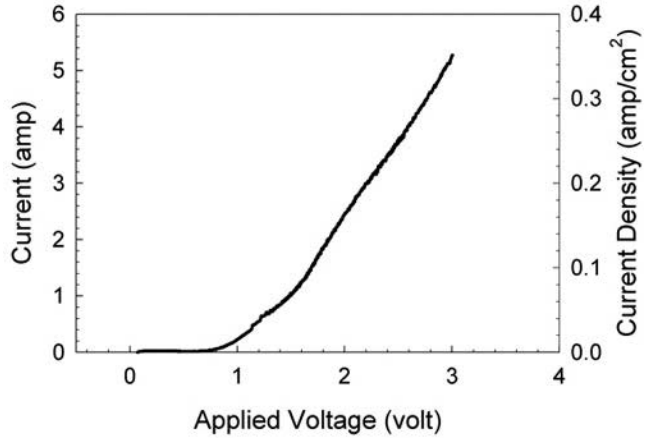

Fig. 9—Fast potentiodynamic scan (5 mv/s) in the LTF system.

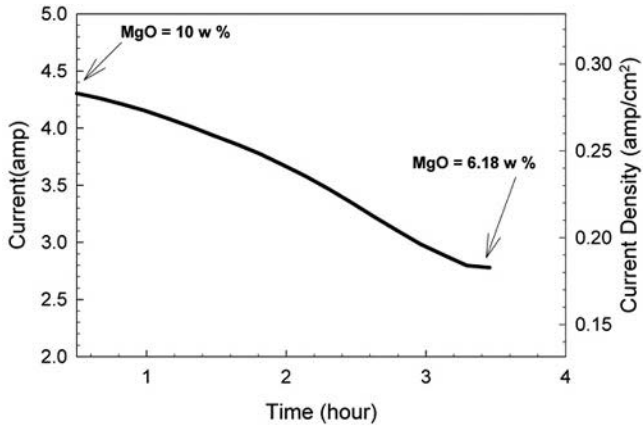

Fig. 10—Current response during electrolysis with 3 V in the LTF system.

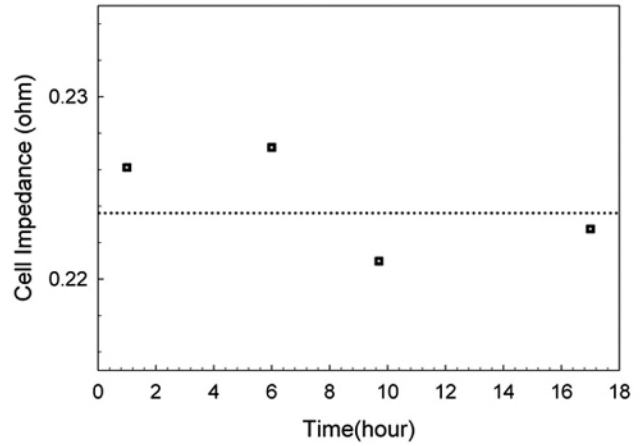

Fig. 11—Periodic impedance measurements of the cell in the LTF system (the dotted line indicates the average of the measured impedance).

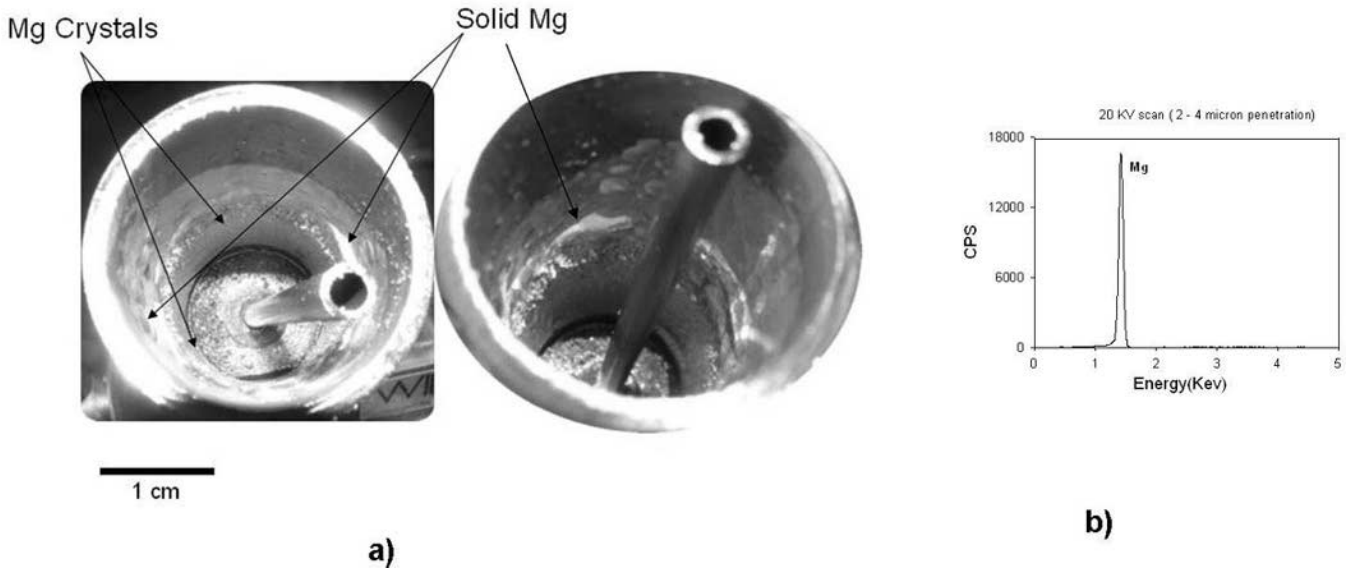

Fig. 12—(*a*) The magnesium deposit inside the condenser and (*b*) chemical analysis (EDAX) of the magnesium deposit in the LTF system.

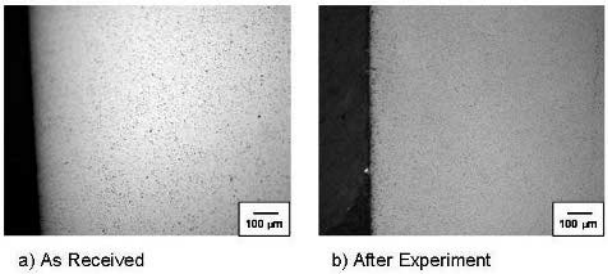

Fig. 13—Cross section of YSZ membrane (*a*) before and (*b*) after the experiment.

C. *Leakage Current*

During a slow potentiodynamic sweep, small current was observed below the MgO dissociation potential. In this section, the origin of this leakage current in terms of various cell variables and its impact on the overall process is discussed.

1. *Origin of leakage current*

Relevant to the transport in the SOM cell are the molten fluoride–based supporting electrolyte containing the dissolved metal oxide, YSZ membrane, and liquid copper as an extended anode. Magnesium fluoride is a pure ionic conductor and YSZ has both oxygen ionic and electronic conductivities (dependent on temperature and P_{O_2}). Liquid copper, apart from being an electronic conductor, has high solubility for oxygen ($[O]_{cu}$). Magnesium fluoride is an electron blocker and YSZ allows only oxygen ions to migrate. Therefore, any current that flows through the cell is solely as a result of the transport of O^{2-}. This is further discussed later in the paper while describing the equivalent circuit of the SOM cell. Consider the case of a potentiodynamic sweep where the electrical potential between the cathode and the anode is increased at a constant rate. When the potential between the anode and cathode exceeds the dissociation potential for magnesium oxide dissolved in the flux, oxygen ions are transported through the flux and YSZ to the anode where they are oxidized. Simultaneously magnesium ions are transported to the cathode and, upon reduction, result in the evolution of magnesium vapor. Ideally, there should be no current until the dissociation potential of magnesium oxide is reached. The nature of the I-V plot after the dissociation potential is a function of mass transfer in the system and is discussed later. The current observed before the dissociation potential (Figure 8) has to be due to ionic transport of oxygen ions. In the ionic melt, the dissolved magnesium oxide exists as associated ions of Mg and oxygen, and they take part in the reaction only when the dissociation potential is reached. Hence, there must be other sources of oxygen ions that are responsible for the current before the dissociation potential is reached. There are two possible sources.

a. *Oxygen in the gas phase above the flux*

Although high-purity argon is used to maintain an inert gas environment in the SOM cell, it has a finite oxygen partial pressure ($P_{O_2} = 10^{-17}$ to 10^{-20} atm), as measured in the exit gas by a zirconia oxygen sensor. This is especially noticeable prior to the evolution of magnesium vapor from MgO dissociation. The reduction of the trace oxygen impurity in the gas phase can be expressed by Eq. [3].

$$\frac{1}{2}\,O_2\,(g) + 2e^- = O^{2-} \qquad [3]$$

This reaction occurs at the cathode and is dependent on the partial pressure of oxygen at the cathode ($P_{O_2(\text{cathode})}$), and cathode area. This reaction too will have a certain dissociation potential. It is likely that the potential is very close to the open circuit voltage (OCV) of the cell.

b. *Oxygen solubility in flux*

The flux will have a finite solubility for oxygen and there will be a chemical potential of oxygen in the flux ($\mu_{O_2(\text{flux})}$). In a stagnant flux, the $\mu_{O_2}^{(\text{flux})}$ will not be in equilibrium with the chemical potential of oxygen in the gas ($\mu_{O_2(\text{gas})}$) above the flux. However, in the case of gas-stirred melts, the $\mu_{O_2(\text{flux})}$ will likely be closer to that in the gas phase ($\mu_{O_2(\text{gas})}$). The oxygen dissolved in the flux in the vicinity

of the cathode will undergo reduction to oxygen ions by the reaction similar to Eq. [3].

Thus, the leakage (trickle) current (i_t) can be attributed to two oxygen sources: (1) oxygen in the gas phase and (2) soluble oxygen in the flux and can be expressed by Eq. [4].

$$i_t = k_g \mu_{O_{2(gas)}} + k_f \mu_{O_{2(flux)}} \quad [4]$$

where k_g and k_f are the gas and flux constants, respectively, and they depend on temperature, flux composition, and cathode area.

2. *Experimental setup*

Two flux systems, F1: (MgF_2 + 10 wt pct MgO) and F2: ({60 wt pct CaF_2-MgF_2}-10 wt pct-MgO), were investigated at 1300 °C and 1150 °C, respectively, to understand the leakage current-potential behavior of the cell. The experimental cell (Figure 14) consisted of a steel crucible (5-cm i.d.) containing about 187 g of the flux resulting in a molten flux height of approximately 2.54 cm. A closed one end YSZ tube (1.9-cm-o.d., 1.42-cm i.d., 20-cm long) was held 1.27 cm from the crucible bottom and insulated from the steel end cap with alumina sleeves. The electrical connection to the YSZ membrane was made by a graphite electrode (0.6-cm o.d.) and copper (extended anode) placed inside the membrane. The crucible was cathode 1, an insulated iron rod (0.03-cm o.d.) was cathode 2, and the steel bubbling tube (0.635-cm o.d., 0.46-cm i.d.) served as cathode 3. Ultra-high-purity argon was passed through the steel tube (cathode 3) and it was possible to position it either above or immersed in the flux. This was done either to stir the melt or to set the P_{O_2} above the melt with argon. Another identical steel tube was used to flow humidified forming gas ((Ar + 5 pct H_2) + x pct H_2O) above the cell and set the P_{O_2} above the melt. A zirconia-based oxygen sensor connected in line with the exit gas was used to verify and monitor P_{O_2} of the argon and humidified forming gas. A potentiodynamic sweep (1 mv/s) was applied across the cathode and anode to obtain the current potential behavior. For all scans, the OCV of the cell was allowed to equilibrate before starting the scan. The trends in the leakage current measured in systems F1 and F2 were almost identical except that the magnitude of current in F1 was slightly higher than F2.

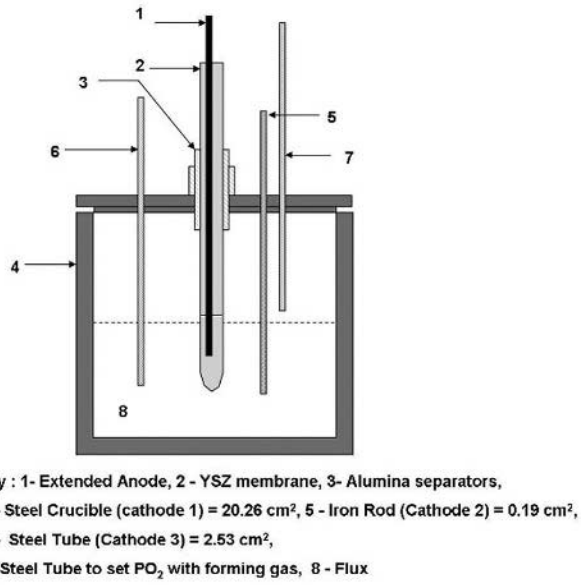

Fig. 14—Experimental setup for leakage current experiments.

3. *Effect of cathode area*

For F1, the P_{O_2} set at cathodes 1, 2, and 3 by humidified forming gas was 5×10^{-12} atm. The effect of cathode area under identical conditions is seen from Figure 15. The area of cathode 1 was 8 times the area of cathode 2 and 100 times the area of cathode 3. However, a linear dependence between cathode area and trickle current is not observed. For small cathode areas such as cathodes (2, 3), as the potential increases, the current also increases. However, for larger cathode areas such as cathode 1, larger currents are observed, but the current seems to plateau after 0.2 V, indicating a diffusion-limited behavior in the oxygen transport.

4. *Effect of cathode P_{O_2}*

For F1, P_{O_2} at the cathode/melt interface was established using buffered compositions of forming gas (Figure 16). Though the difference in P_{O_2} was only an order of magnitude, the effect of cathode P_{O_2} is clearly observed. Therefore, by lowering the cathode P_{O_2}, and decreasing the cathode area, it is possible to decrease the leakage current.

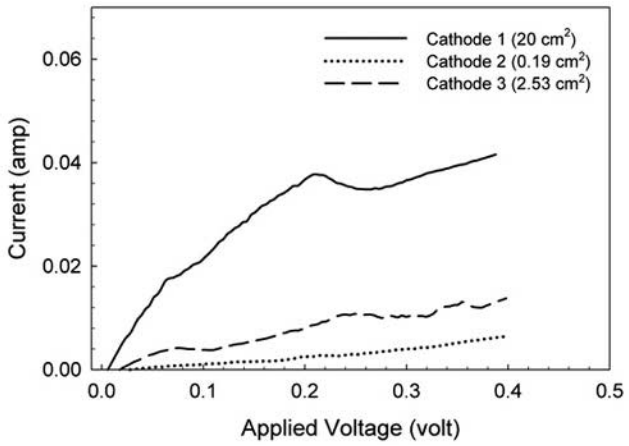

Fig. 15—Effect of cathode area on leakage current in F1.

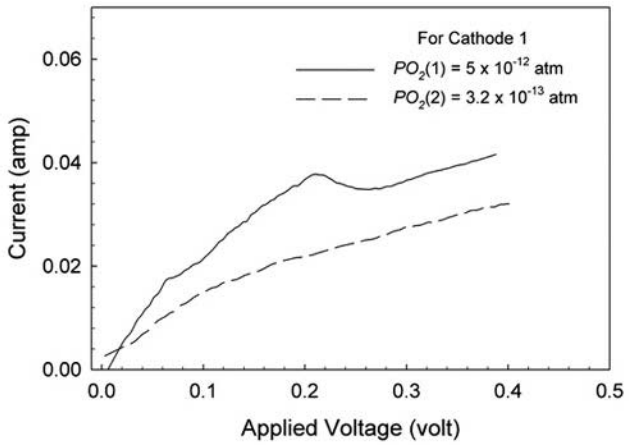

Fig. 16—Effect of P_{O_2} at the cathode/melt interface on leakage current in F1.

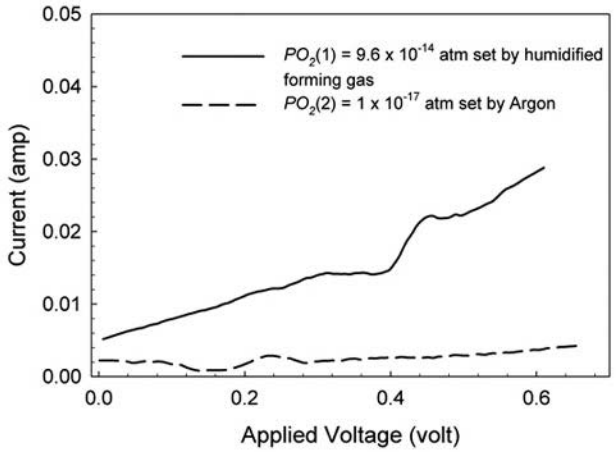

Fig. 17—Effect of $P_{O_2\ (flux)}$ on leakage current in F2.

5. *Effect of flux* P_{O_2}

For F2, in order to establish the P_{O_2} inside the flux, the flux was stirred with gas having known P_{O_2} (P_{O_2} (1) = 9.6 × 10^{-14} atm and P_{O_2} (2) = 10^{-17} atm). Using a constant flow rate of 280 cc/min, the flux was allowed to equilibrate for 30 minutes before starting the scan. Using identical cathodes, it can be seen that the leakage current is larger for the flux when stirred with a gas having a higher P_{O_2} (Figure 17).

6. *Effect of leakage current on SOM process*

It has been established that the very small leakage current in the cell prior to the MgO dissociation is due to oxygen impurity in the cell. Consider the cathodic reaction Eq. [3]:

$$\frac{1}{2}\,O_2\,(g) + 2e^- = O^{2-}$$

The leakage current at low applied potentials, less than the MgO dissociation potential (<0.5 V), will decrease as cathode area and oxygen impurity concentration of the cell are decreased. This is applicable to both flux systems under investigation. However, well above the dissociation potential (>2 V), the dominant cathodic reaction is

$$Mg^{2+} + 2e^- = Mg(g) \qquad [5]$$

With magnesium gas in the cell environment, the trace oxygen impurity will further decrease and the leakage current contribution to the total current will essentially be insignificant. Therefore, during the actual SOM experiments at 4 to 5 V, the contribution of the residual leakage current to the total current will be negligible.

IV. MASS-TRANSFER ANALYSIS

As the applied potential is increased beyond the dissociation potential of magnesium oxide in the flux, magnesium ions are reduced at the cathode ($Mg^{2+} + 2e^- \rightarrow Mg(g)$) and the oxygen ions are transported through the YSZ membrane and oxidized at the Cu(l)/YSZ interface ($O^{2-} \rightarrow [O]_{Cu} + 2e^-$). The dissolved oxygen in the Cu(l) is then transported to the carbon (graphite) current collector, where it chemically reacts to form CO(g). Since the flux is essentially a fluoride-ion conductor (supporting electrolyte), the oxygen ion transport through the flux must be diffusive in nature. Since the flux is an electron blocker, the current passing through the cell (I_{cell}) is purely ionic, and under the condition that the flux remains electrically neutral and that no accumulation of oxygen occurs in the cell, the individual fluxes (J) can be expressed by Eqs. [6] and [7].

$$J_{mg^{2+}} \times A_{cathode} = J_{O^{2-}} \times A_{flux/YSZ} = J_{[O]_{Cu/YSZ}} \times A_{Cu/YSZ} = J_{[O]_{Cu/C}} \times A_{Cu/C} = \frac{I_{cell}}{2F} \qquad [6]$$

or

$$D_{Mg^{2+}}\left[\frac{(C^b_{Mg^{2+}} - C^i_{Mg^{2+}})}{\delta_{cathode/flux}}\right]A_{cathode} = D_{O^{2-}}\left[\frac{(C^b_{O^{2-}} - C^i_{O^{2-}})}{\delta_{flux/YSZ}}\right]A_{flux/YSZ} = D_{[O]_{Cu}}\left[\frac{(C^i_{[O]_{Cu/YSZ}} - C^b_{[O]_{Cu}})}{\delta_{YSZ/Cu}}\right]A_{YSZ/Cu} = D_{[O]_{Cu}}\left[\frac{(C^b_{[O]_{Cu}} - C^i_{[O]_{Cu/C}})}{\delta_{Cu/C}}\right]A_{Cu/C} \qquad [7]$$

where D, C^b, C^i, δ, and A represent the diffusivity, bulk concentration, interfacial concentration, boundary layer, and area, respectively. The applied electric potential ($E_{applied}$) can be expressed in terms of the oxygen chemical potential (μ_O) between the electrodes (stainless steel cathode and the liquid copper anode) as

$$E_{applied} = I_{cell}R_{total} + \frac{\mu_{O(anode)} - \mu_{O(cathode)}}{2F} \qquad [8]$$

where the Nernst potential established between the electrodes (E_N),

$$E_N = \frac{\mu_{O(anode)} - \mu_{O(cathode)}}{2F} \qquad [9]$$

and

$$I_{cell}R_{total} = I(R_{mt} + R_{ohmic}) \qquad [10]$$

In Eq. [10], the mass-transfer resistance in the cell is represented by R_{mt} and the total ohmic resistance of the cell by R_{ohmic}. It is assumed that the charge transfer resistance is negligibly small at these temperatures.[40] R_{ohmic} is essentially the sum of the ionic resistances of the flux (R^i_{flux}), and the YSZ membrane (R^i_{YSZ}) and resistance of the electrodes and lead wires ($R_{external}$).

$$R_{ohmic} = R^i_{flux} + R^i_{YSZ} + R_{external} \qquad [11]$$

The flux is a known ionic electrolyte, it blocks electronic current, and it has a very high electronic resistance (R^e_{flux}). As the oxyfluoride flux is in series with the zirconia membrane, there is no electronic current flow through the zirconia membrane. The electronic resistances of the flux and the YSZ membrane (R^e_{flux} and R^e_{YSZ}) do not contribute to R_{ohmic}. The equivalent circuit representing all the potentials and the resistive elements are shown in Figure 18. It is to be noted that reducing conditions cause the zirconia to lose oxygen and become nonstoichiometric ($ZrO_{2-\delta}$). This does induce n-type

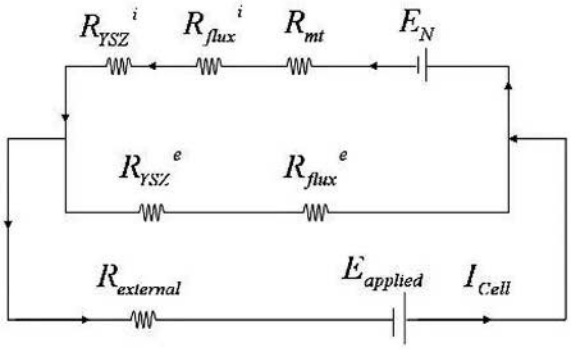

Fig. 18—Equivalent circuit of the SOM cell.

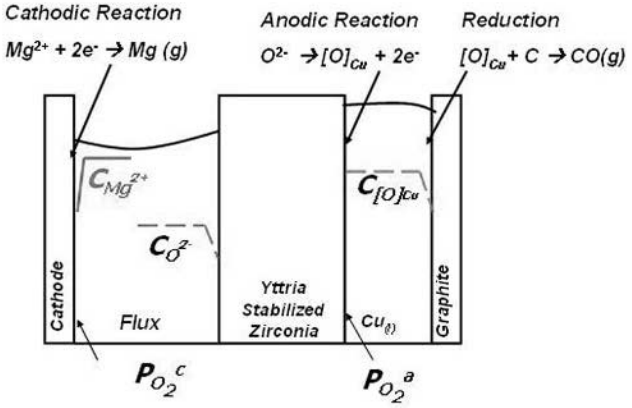

Fig. 19—Expected concentration gradients in the SOM cell.

conduction in zirconia. However, since the oxygen ion conductivity in zirconia is known to be independent of the oxygen chemical potential and the oxy fluoride flux blocks the electrons, the current through the system is all due to oxygen ions. This also agreed with the observation that the amount of magnesium collected is 100 pct Faradic equivalent of the total current. The applied potential (E_{applied}) overcomes the Nernst potential (E_N) established across the electrodes to dissociate the MgO and transport the oxygen ions, and results in an ionic current depending on R_{ohmic} and R_{mt}.

The chemical potential of oxygen at the cathode ($\mu_{\text{O(anode)}}$) is established by the reaction MgO = Mg (g) + $\frac{1}{2}$ O_2(g) and is expressed by Eq. [12].

$$\mu_{\text{O(cathode)}} = \mu_{\text{MgO}} - \mu_{\text{Mg(g)}} = \frac{1}{2}\text{R}T \ln P_{\text{O}_2\text{(cathode)}} + \mu_{\text{O}}^{o} \quad [12]$$

Similarly, the chemical potential at the anode can be expressed as

$$\mu_{\text{O(anode)}} = \frac{1}{2}\text{R}T \ln P_{\text{O}_2}(\text{anode}) + \mu_{\text{O}}^{o} = \mu_{[\text{O}]_{\text{Cu/YSZ}}} \quad [13]$$

where μ_{O}^{o} is the standard oxygen chemical potential.

The chemical potential of oxygen in Cu(l) at the carbon/Cu(l) interface is established by the C/CO reaction, and

$$\mu_{[\text{O}]_{\text{C/Cu}}} = \mu_{\text{CO(g)}} - \mu_{\text{C}} \quad [14]$$

Since the C solubility in Cu(l) is negligible, the gradient of the oxygen chemical potential in Cu(l) (dissolved oxygen concentration) will depend on the mass-transfer coefficient of dissolved oxygen in Cu(l) $\left(\frac{D_{[O]Cu}}{\delta}\right)$ and the relative areas of the YSZ/Cu(l) and C/Cu(l) interfaces (refer Eq. [6]). If we assume that the interfacial area of the YSZ/Cu(l) interface is much larger than the interfacial area of the Cu(l)/C interface (as in the case of the discussed experiments), then the major drop of the oxygen chemical potential gradient will occur at the C/Cu(l) interface. In other words, the dissolved oxygen concentration in Cu(l) at the YSZ/Cu(l) interface will be the same as that in bulk Cu(l) and the dissolved oxygen concentration will drop near the Cu(l)/C interface. If we know the mass-transfer coefficient of dissolved oxygen in Cu(l) (between 1150 °C to 1300 °C, it is expected to be in the range 0.01 to 0.1 cm/s[20]), the oxygen flux, and the relative areas of the YSZ/Cu(l) and the C/Cu(l) interfaces, we can calculate the dissolved oxygen concentration or the oxygen chemical potential at the Cu/YSZ interface (From Eqs. [2] and [7]). The expected variation of various species in the system is schematically shown in Figure 19. It should be noted that in Figure 19, different standard states have been used in order to visualize the gradients of various species that exist in the system. The oxygen concentration at the electrodes is represented by the oxygen partial pressure, and in the flux and liquid copper by oxygen ion ($C_{O_{2-}}$) and dissolved oxygen ($[\text{O}]_{\text{Cu}}$) concentrations, respectively.

From Eq. 8, it is possible to write

$$E_N = E_{\text{applied}} - I_{\text{cell}}R_{\text{total}} = \frac{\mu_{O(\text{anode})} - \mu_{O(\text{cathode})}}{2F} = \frac{\text{R}T}{4F} \text{In}\left(\frac{P_{\text{O}_2\text{(anode)}}}{P_{O_2\text{(cathode)}}}\right) \quad [15]$$

It is clear that $E_{\text{applied}} = E_N$ at the dissociation potential of the magnesium oxide in the flux since $I_{\text{cell}} = 0$. At higher applied potentials, depending on the mass transfer in the flux, E_N will either increase with E_{applied} or remain the same. This implies that $\frac{\partial E_{\text{applied}}}{\partial I} \geq R_{\text{total}}$ at all times. Since the plot of E_{applied} versus I (Figure 9) does not show a diffusion-limited behavior, it is possible to get an upper estimate of R_{total} from the inverse of the slope of the linear region of the plot. The AC impedance spectroscopy was used to determine R_{ohmic} in the system (Figure 11), and by subtracting it from the upper estimate of R_{total}, it was possible to get an upper estimate of the mass-transfer resistance (R_{mt}) in the cell. These measurements showed that in a well-stirred SOM cell system, for instance, in LTF at 1150 °C, R_{mt} was less than 0.1 ohms while R_{ohmic} was around 0.3 ohms. This indicates that mass transfer in the flux is not rate limiting, and it is possible to obtain higher current densities with larger E_{applied}. This agrees with the fact that diffusion-limited behavior is not observed in E_{applied} *vs* I_{cell} plots (Figures 5 and 9).

It should be noted that the success of the SOM process is highly dependent on the selection of the flux. Since high potentials are applied to obtain high current densities, it is extremely important to make sure that there is no dissolution of the oxides (ZrO_2 and Y_2O_3) from the membrane into the flux. Otherwise, those oxides are likely to be reduced at the cathode and the dissolution may continue. It is desirable

for the flux to have little or no solubility for the membrane material. The selected flux system was tailored to limit dissolution of ZrO_2 and Y_2O_3 from the membrane. The cross section of the YSZ membrane before and after a 20-hour SOM run at 0.3 A/cm^2 is shown in Figure 13. It can be seen that the membrane structure remains virtually unaltered. This is an important consideration for scaleup since the YSZ membrane is expected to be one of the most expensive parts of the SOM cell and its life is likely to dictate process economics. Problems regarding thermal shock and mechanical failure of zirconia membranes are also additional engineering challenges. However, researchers working in the area of SOFCs with zirconia membranes have overcome these challenges and are able to successfully operate SOFC systems for longer durations (>5 years). During future scale-up investigations of the SOM process, these additional challenges pertaining to thermal shock and mechanical failure will be addressed.

V. CONCLUSIONS

Magnesium has been produced directly from magnesium oxide using the SOM process. Two flux systems, HTF: {MgF_2-10 wt pct MgO} at 1300 °C and LTF: {(55.5 wt pct MgF_2-CaF_2)-10 wt pct MgO} at 1150 °C), have been successfully used to demonstrate proof of concept for this process. The dissociation potential of MgO in the above flux systems was between 0.59 to 0.63 V. Magnesium produced by the SOM process is free of impurities since the deposit is condensed from magnesium vapors. A decrease in operating temperature achieved by the low-temperature flux system is seen as an improvement for eventual commercialization of this process. High current densities (>1 A/cm^2) for electrolysis are possible by increasing the applied electrical potential. Also, with proper flux selection, the membrane has been observed to be virtually unaffected by the SOM process. Both these attributes are strong indicators that the SOM process is viable and has excellent scale-up potential for Mg production. The oxygen impurity in the cell has been identified to be responsible for the observed leakage current. However, its effect on the overall efficiency of the process is insignificant. The mass transfer in the cell is explained using an equivalent circuit model.

The SOM process is a generic process for extraction of high energy content metals. The knowledge gained from the magnesium SOM process can be applied to extraction of other important and difficult to extract metals such as tantalum, titanium, niobium, and chromium.

ACKNOWLEDGMENTS

The authors thank Safe Hydrogen LLC and the Department of Energy (DOE) for funding this research through Award No. DE-FC36-04GO14011 and Contract No. C407200-AN8. Such support on the part of DOE does not constitute an endorsement by DOE of the views expressed in this article. The assistance of Dr. Chris Manning with performing some of the experiments and Robert Sjostrom with fabrication of experimental setups is greatly appreciated.

REFERENCES

1. D. Kramer: U.S. Geological Survey Report No. 01-341, Reston, VA, 2001, pp. 1-30.
2. F. Froes, D. Eliezer, and E. Aghion: *J. Met*., 1998, Sept., pp. 30-34.
3. A. McClaine, K. Brown, and S. Tullmann: *Fuel Cells*, 2003 (2003).
4. D. Woolley, U. Pal, and G. Kenney: *J. Met*., 2001, Oct., pp. 32-35.
5. N. Kanari and I. Gaballah: *Metall. Mater. Trans. B*, 1999, vol. 30, pp. 383-91.
6. T.H. Okabe, M. Nakamura, T. Oishi, and K. Ono: *Metall. Trans. B*, 1993, vol. 24B, pp. 449-55.
7. T.H. Okabe, T.N. Deura, T. Oishi, K. Ono, and D. Sadoway: *J. Alloys Compounds*, 1996, vol. 237, pp. 150-54.
8. G. Chen and D. Fray: *J. Appl. Electrochem*., 2001, vol. 31, pp. 155-64.
9. D.J. Fray, G.J. Chen, and T. Farthing: *Nature*, 2000, vol. 407, pp. 361-64.
10. R. Suzuki and K. Ono: *Metall. Trans. B*, 2003, vol. 34B, pp. 287-95.
11. X. Van and D. Fray: *Metall. Trans. B*, 2002, vol. 33B, pp. 685-93.
12. C. Chen, E. Gordo, and D. Fray: *Metall. Mater. Trans. B*, 2004, vol. 35B, pp. 223-33.
13. X. Jin, P. Gao, D. Wang, X. Hu, and G. Chen: *Angewandte Chemie*, 2004, vol. 43, pp. 733-36.
14. K. Kiukkola and C. Wagner: *J. Electrochem. Soc*., 1957, vol. 104, pp. 308-16.
15. W. Fischer and D. Janke: *Scripta Metall*., 1972, vol. 6, pp. 923-28.
16. B. Korousic and B. Marincek: *Helvetica Chimica Acta*, 1968, vol. 51, pp. 907-11.
17. K.E. Oberg, W.M. Boorstein, and R.A. Rapp: *Metall. Trans*., 1973, vol. 4, pp. 75-82.
18. M. Iwase, M. Tanida, A. McLean, and T. Mori: *Metall. Trans. B*, 1981, vol. 12B, pp. 517-24.
19. Z. Hasham, U. Pal, K.C. Chou, and W.L. Worrell: *J. Electrochem. Soc*., 1995, vol. 141, pp. 469-75.
20. S. Yuan, U. Pal, and K. Chou: *J. Am. Ceram. Soc*., 1996, vol. 79, pp. 641-50.
21. J. Kummer: U.S. Patent No. 3,488,271, Jan. 6, 1972.
22. R. Minck: U.S. Patent No. 4,108,743, Aug. 22, 1978.
23. B. Marincek: U.S. Patent No. 3,692,645, Sept. 19, 1972.
24. B. Marincek: U.S. Patent No. 3,562,135, Feb. 9, 1971.
25. A. Sammells: U.S. Patent No. 4,804,448, Feb. 14, 1989.
26. U. Pal and S. Britten: U.S. Patent No. 5,976,345, Nov. 2, 1999.
27. U. Pal and S. Britten: U.S. Patent No. 6,299,742, Oct. 9, 2001.
28. U. Pal, K. Chou, S. Yuan, and Z. Hasham: U.S. Patent No. 5,567,286, Oct. 22, 1996.
29. R.A. Rapp: U.S. Patent No. 5,942,097, Aug. 24, 1999.
30. R.A. Rapp: U.S. Patent No. 6,039,862, Mar. 21, 2000.
31. R. Rapp and Y. Zhang: *Light Metals*, TMS, Warrendale, PA 2002, pp. 469-74.
32. A. Lacamera: U.S. Patent No. 6,187,168, Feb. 13, 2001.
33. D. Poa: U.S. Patent No. 4,995,948, Feb. 26, 1991.
34. K.E. Oberg, W.M. Boorstein, and R.A. Rapp: *Metall. Trans*., 1973, vol. 4, pp. 61-67.
35. A. Roine: *HSC Thermodynamic Software*, 5th ed., Outokumpo Research Oy, Pori, Finland, 2003.
36. U.B. Pal, D.E. Woolley, A. Krishnan, T. Keenan, C.P. Manning, and G.B. Kenney: *TMS Magn. Technol*., 2002, pp. 19-24.
37. J. Berak and I. Tomczak: *Roczniki Chemii*, 1965, vol. 39, pp. 519-28.
38. J. Macdonald: *Impedance Spectroscopy: Emphasizing Solid Materials and Systems* (New York: John Wiley, 1987).
39. E. Beck: *Metallurgie*, 1908, vol. 5, pp. 504-08.
40. S. Britten and U. Pal: *Metall. Mater. Trans. B*, 2000, vol. 31 B, pp. 733-53.